Radiative double-electron capture by fully stripped and one-electron ions in gas and thin-foil targets

J. A. Tanis ,* D. S. La Mantia , and P. N. S. Kumara
Department of Physics, Western Michigan University, Kalamazoo, Michigan 49008, USA

(Received 28 February 2021; accepted 17 August 2021; published xxxxxxxxxx)

Radiative double-electron capture (RDEC), in which two-electron capture is accompanied by simultaneous emission of a single photon, was investigated for fully stripped and one-electron projectiles colliding with gaseous and thin-foil targets. RDEC can be considered the inverse of double photoionization by a single photon. For the gaseous targets, measurements were done for 2.11 MeV/u F^{9+} and F^{8+} ions interacting with N_2 and Ne, while for the thin-foil target the measurements were done for 2.11 MeV/u F^{9+} and F^{8+} and 2.19 MeV/u O^{8+} and O^{7+} ions striking thin C targets. Reports on this work were already published separately in shorter accounts by La Mantia *et al.* [Phys. Rev. Lett. **124**, 133401 (2020) for the gas targets and Phys. Rev. A **102**, 060801(R) (2020) for the thin-foil targets]. The gas targets were studied under single-collision conditions, while the foil targets suffered unavoidable multiple collisions. The measurements were carried out by detecting x-ray emission from the target at 90° to the beam direction in coincidence with outgoing ions undergoing double, single, and, in the case of the foil targets, no charge change inside the target. Striking differences between the gaseous and foil targets were found from these measurements, with RDEC for the gaseous targets occurring only in coincidence with q-2 outgoing projectiles as expected, while RDEC for the foil targets was seen in each of the outgoing q-2, q-1, and no charge-change states. The no charge-change result was totally unexpected. The cross sections for RDEC for the fully stripped ions on gas targets were found to be about six times larger than those for the one-electron projectiles. For the foil targets, the RDEC cross sections for the fully stripped and one-electron projectiles differ somewhat from one another but not to the the extent they did for the gas targets. In this work the cross sections for all of the projectiles for the foil targets were adjusted due to the target contaminant background from potassium and calcium atoms that existed in the spectra. Also, the cross sections for the incident one-electron projectiles were modified due to a correction for the fraction of these ions that becomes fully stripped in passage through the foil. These differences are attributed to the effects of the multiple collisions that occur for the foil targets. The differential cross sections at 90° determined for each of the projectiles interacting with each of the targets are compared with each other and with the previous measurements. To the extent that the cross sections follow a $\sin^2\theta$ dependence, the total cross sections are compared with theoretical calculations [E. A. Mistonova and O. Yu. Andreev, Phys. Rev. A **87**, 034702 (2013)], for which the agreement is poor, with the measured cross section exceeding the predicted ones by about an order of magnitude. Possible reasons for this discrepancy will be discussed.

DOI: 10.1103/PhysRevA.00.002800

I. INTRODUCTION

Recently, in two papers, we published our findings for radiative double-electron capture (RDEC) by fully stripped and one-electron ions moving through gas [1] and thin-foil targets [2]. The collisions were investigated with the experimental results for gas and foil targets compared with each other and with available theoretical calculations. The measurements, which were difficult and time consuming, provided the first unambiguous evidence for the existence of RDEC, a process that can be considered the inverse of double photoionization.

Electron capture by highly charged ions moving in matter consisting of gases, solids, and plasmas is of fundamental and applied interest, including astronomical aspects. This interest is continually studied in all three matter states, both experimentally and theoretically. Of the several processes that are possible, electron capture simultaneous with the emission of a single photon is of particular challenging interest. In the case of interest here, this capture occurs as a single or double event. In the former case, the process is called radiative electron capture (REC) [3–5] if the capture comes from a bound atomic or molecular electron and is referred to as radiative recombination for a free electron. Either of these processes (free or bound electrons) can be considered the inverse of single photoionization. For the case of two electrons captured with emission of a single photon, the process is called radiative double-electron capture (RDEC) [6] when the electrons are both initially bound. Here, the process is considered as the inverse of double photoionization by a single photon. Hence, radiative double-electron capture is intimately connected with its inverse process and should provide insight into it. Incidentally, double ionization between a single photon and a two-electron ion is not currently measurable for an atomic system other than atomic helium due to the technical difficulties of obtaining beams of photons and ions with sufficient intensity to carry out these investigations.

So far, studies of RDEC occurring in ion-atom and molecule collisions have been quite sparse due to the

*john.tanis@wmich.edu

complicated experimental setups and the rather long times required to obtain sufficient and accurate data (measurements to date have taken about three weeks of round-the-clock data acquisition for a single projectile-target gas system). Despite these difficulties, RDEC has been investigated experimentally in six trials over the past two and a half decades. The first measurement was reported in 1995 for 11.4 MeV/u Ar^{18+} on C [7], followed by measurements reported in 2003 for 297 MeV/u U^{92+} on Ar [8]. Neither of these studies, conducted at the GSI facility in Germany, showed evidence of RDEC. In 2010, from measurements done at Western Michigan University with the tandem Van de Graaff accelerator, following the suggestion of Nefiodov *et al.* [9] that lower-energy, mid-Z ions may lead to larger RDEC probabilities, some evidence for RDEC from measurements for 2.4 MeV O^{8+} on C [10] was seen, followed by measurements in the same laboratory for positive RDEC results for 2.2 MeV/u F^{9+} striking C [11]. These studies were followed by additional work done at GSI reported for 30 MeV/u Cr^{24+} ions on He and N_2 targets [12] that again showed no evidence of RDEC. This body of work represents the extent of experimental RDEC investigations that were completed until the work reported here.

In this paper, we report results of studies of RDEC for fully stripped and one-electron $F^{9,8+}$ ions on gas targets of N_2 and Ne, and the same for $O^{8,7+}$ and $F^{9,8+}$ ions incident on thin-foil C targets. For the thin-foil targets there is the expectation that charge changing of the incident ion occurs after it undergoes capture (and the RDEC process) and continues its passage through the foil. Our recent successful works on RDEC are combined in this paper, bringing together the similarities and differences between RDEC in gas and thin-foil targets. For gas targets done under single-collision conditions, the RDEC results show the expected behavior with the events occurring only for ions that have captured two electrons, while for the thin-foil targets it is found that RDEC occurs for all three outgoing charge states of q-2, q-1, and q. These outcomes due to RDEC in foils are a result of the unavoidable multiple charge-changing collisions as the ions pass through the foil. Also, the probabilities for RDEC in fully stripped projectiles incident on the gas targets were found to be about six times larger than those for incident one-electron projectiles. For the foil targets, a difference of a factor of 6 was not seen, with the fully stripped and one-electron projectiles showing much more comparable probabilities. Significant differences are found in the experimental cross sections of the outgoing charge states between oxygen and fluorine ions, despite their differing by only one atomic number. The cross sections for RDEC will be compared with each other and the results for gas targets will be compared with those obtained for the thin-foil targets. Finally, the cross sections will be compared with available theoretical cross sections to the extent possible. These, as well as other RDEC features, will be discussed in detail in this paper.

II. KINEMATIC CONSIDERATIONS

As the starting point of our consideration of RDEC, Fig. 1 shows the schematics of single-electron capture REC and double-electron capture RDEC of interest here. In these processes, one (REC) or two (RDEC) electrons from bound states

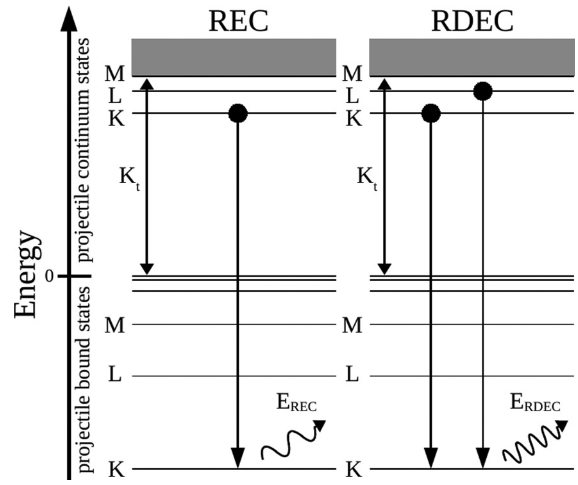

FIG. 1. Energy diagram showing the (a) REC and (b) RDEC processes. In REC, one electron is captured from a target bound state to the projectile with simultaneous emission of a single photon. In RDEC, two electrons are captured from target bound states to the projectile with the simultaneous emission of a single photon. Generally, the electrons can be captured from any target bound states to any bound states of the projectile.

of the target atom are transferred to the projectile accompanied by the simultaneous emission of a single photon. For REC there are two possible transitions while there are six for RDEC, in which an electron(s) from the target fills at least one vacancy in the K shell of the projectile. It is only these K-populating states that can be observed in this work. To get the REC or RDEC energy of the emitted photon, the kinetic energy K_t of the captured electron, as seen from the rest frame of the projectile, must be added to this energy. To this must be added or subtracted the binding energies in the projectile B_p and the target B_t, and a term representing the Compton profile [13] of the captured electrons along the beam direction, resulting in a broadening of the transition peak. From the energy schematics for REC and RDEC shown in Fig. 1, the energies of the REC and RDEC photons emitted can be written as

$$E_{\mathrm{REC}} = K_t + B_p - B_t + \vec{v}_p \cdot \vec{p}_{it}, \tag{1}$$

$$E_{\mathrm{RDEC}} = 2K_t + B_p^1 + B_p^2 - B_t^1 - B_t^2 + \vec{v}_p \cdot \vec{p}_{it}^{\,1} + \vec{v}_p \cdot \vec{p}_{it}^{\,2}. \tag{2}$$

In these equations the binding energies (the B values) are taken as positive, and the quantities v_p and p_{it} represent, respectively, the velocity of the projectile ion in the laboratory frame and intrinsic momentum of the captured electron due to its orbital motion in the target atom. The Compton profile is recognized as having rather large influences on the peak widths due to RDEC in the x-ray spectrum. Generally, it has been assumed the Compton profile broadens the peaks by about a factor of 2, although this broadening has not been verified because the statistics obtained so far for any of the RDEC x-ray peaks are insufficient to show this. However, the effect of this broadening has definitely been shown for REC peaks that were observed (see, for example, Ref. [4], Fig. 9). In general, the target electrons can be captured to the same

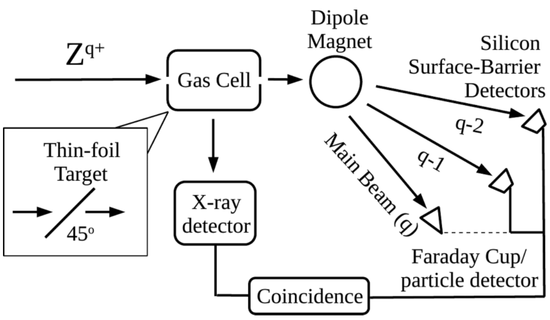

FIG. 2. Schematic diagram of the experimental setup. For the gas targets the setup is that shown in the main part of the figure with gas cell placed in the beam line. To measure the thin-foil targets, the gas cell is removed and the setup shown as the inset in the lower left of the figure is installed in the beam line.

or different bound states of the projectile, with each possible transition emitting a photon corresponding its distinct energy.

Another point to consider in determining the total RDEC cross sections is the relationship between the usually observed differential cross sections (at 90°) and the total cross sections. For REC this relationship has a $\sin^2\theta$ dependence [14,15] resulting in the following connection between the measured cross section at 90° and the total cross section:

$$\sigma_{\text{REC}}^{\text{total}} = \frac{8\pi}{3}\frac{d\sigma_{\text{REC}}}{d\Omega}(\theta = 90^\circ). \tag{3}$$

In this equation, Ω represents the solid angle seen by the x-ray detector from the point of view of the target. If this same dependence is assumed for RDEC, then the total cross section can be determined from the same equation. It is recognized that a detailed study of the RDEC polarization would be useful, but such an examination of the angular dependence would be quite difficult due to the small cross sections and the time involved in making the measurements. Hence, the expression given by this equation will be used in this paper.

A final point that needs to be considered is the probability for emission of two REC photons detected simultaneously with each event causing the capture of one additional electron. During this simultaneous emission the energy of the two photons will be added in the x-ray detector, appearing as a single photon with about twice the energy equal to the RDEC photon energies [see Eqs. (1) and (2)]. However, the cross section for this double REC process scales as $(\sigma_{\text{REC}}/a_0)^2$ with $\sigma_{\text{REC}} \ll a_0$ [16], making its probability of observation about two orders of magnitude smaller than that for RDEC.

III. EXPERIMENTAL PROCEDURES

The measurements for this work were carried out with the 6-MV tandem Van de Graaff accelerator facility at Western Michigan University. Figure 2 shows a schematic of the experimental setup for both the target gas measurements and those done for the thin-foil carbon targets. The projectile ions, accelerated to $\sim$2 MeV/u, collided with the gas target (cell length $\sim$4 cm, pressure $\sim$10 mTorr $\rightarrow 1.3 \times 10^{15}$ atoms/cm^2) contained inside a differentially pumped cell, or with the carbon target mounted on a holder tilted at 45° to the beam direction. Due to its uncomplicated design, switching between the target gas cell and the target ladder was a simple matter and could be accomplished in about an hour. A Si(Li) x-ray detector was placed at 90° to the beam as shown (asymmetries in the cross sections could not be measured because it was not possible to change the angle of the detector). After passing through the target, the outgoing ions were separated according to charge state using a dipole magnet, and the q-2, q-1, and q charge states were counted with separate surface-barrier detectors. For the measurements with the gas targets, coincidences with the main beam could not be detected due to its high intensity (about 95% of the beam exited the collision region in this charge state), so a Faraday cup was used instead to measure the main beam. Taking data for the gas targets (N_2 and Ne) was a long process, requiring round-the-clock collection times of about three weeks for each projectile charge state and each target. For the carbon target, the Faraday cup was replaced with a solid-state Si particle detector, so all of the outgoing beam fractions were observed, except for O^{8+} and F^{9+} when the initial beams were one-electron ions, and coincidences with the observed fractions recorded. Data were gathered much more quickly for the carbon target due to it being significantly thicker, with each projectile and charge state requiring just two to three days of measuring time. The disadvantage of not counting O^{8+} and F^{9+} for initial beams of O^{7+} and F^{8+} is that the actual fraction of charge-stripped ions is not measured and, hence, the fraction must be calculated from reported values of the cross sections and the number of RDEC photons estimated.

The x-ray detector, with an effective observation area of $\sim$60 mm^2, was positioned at a distance of 1.7 ± 0.1 cm from the target for the gases, while this distance was 2.8 ± 0.1 cm for the C-foil targets, corresponding to detection solid angles of 0.208 and 0.0765 steradians, respectively, for the two target cases. The detection efficiency of x rays with energies in the calculated RDEC energy range is greater than $\sim$98%. For each of the measurements with different projectiles (F^{9+}, F^{8+}, O^{8+}, and O^{7+}), short runs with no gas or an empty foil holder (without the C target) were performed in order to show that no background events contributed to the measurements.

Data acquisition was done using event-mode collection with the coincidences between x rays and particles observed in the q-2, q-1, and q charge states recorded separately (except for the gas targets for which the beam was too intense to measure the no charge change state separately). This allowed the collected data to be analyzed by (1) a gate condition applied to the particle spectra to generate x rays associated with them (referred to as particle-gated x-ray spectra), or (2) a gate condition applied to the x-ray spectrum to generate the particle spectra associated with the individual charge states (referred to as x-ray gated particle spectra). These two methods should be consistent with each other and give similar numbers of events observed for RDEC.

IV. RESULTS

In this work, studies were undertaken for eight different projectile-target systems, specifically, fully stripped and one-electron $F^{9,8+}$ ions incident on gas targets of N_2 and Ne, and for $O^{8,7+}$ and $F^{9,8+}$ ions incident on thin-foil C targets. For the gas targets, helium was also tried but the counting rate was too

TABLE I. Calculated RDEC energies (eV) for electron transitions involving at least one electron going to the projectile K shell for 2.11 MeV/u (40 MeV) $F^{9,8+}$ ions incident on gas targets of N_2 and Ne and for 2.19 MeV/u (35 MeV) $O^{8,7+}$ and 2.11 MeV/u (40 MeV) $F^{9,8+}$ ions incident on thin-foil carbon targets. For the one-electron projectiles, transitions with both electrons going to the K shell are not possible due to there being already an electron in that shell. In the list of electron transitions the designation V refers to valence (quasifree) electrons.

	Projectile-target system							
RDEC electron transition	40 MeV F^{9+}+ N_2	40 MeV F^{8+}+ N_2	40 MeV F^{9+}+ Ne	40 MeV F^{8+}+ Ne	35 MeV O^{8+}+ C	35 MeV O^{7+}+ C	40 MeV F^{9+}+ C	40 MeV F^{8+}+ C
$VV \to KK$	4350		4350		4333		3993	
$VK \to KK$	3940		3480		4056		3716	
$KK \to KK$	3530		2610		3779		3439	
$VV \to KL$	3610	3466	3610	3466	3615	3414	3420	3244
$VK \to KL$	3200	3056	2740	2596	3338	3137	3143	2967
$KK \to KL$	2790	2646	1870	1726	3061	2859	2866	2690

low (three RDEC counts were obtained in 10 days of round-the-clock running) to make this target possible in the allocated beam time. Calculated RDEC energies of the six transitions involving transfer of one or two electrons to the K shell for the eight target-projectile systems are listed in Table I. For the one-electron projectiles O^{7+} and F^{8+}, two electrons from the target atom cannot be captured to the projectile K shell due to the existing electron in that shell. However, transitions with the final state being KL (corresponding to the transfer of one electron to the K shell and the other to the L shell) are possible.

Figures 3 and 4 show the raw spectra (without applying any gates) obtained for the F^{9+}+ N_2 gas and the F^{9+}+ C thin-foil systems. Due to the large difference in counting rates between the x rays (much lower) and the particles, the trigger for the coincidence events was set on the x rays. Therefore, the timescale is somewhat arbitrary because the particle signals had to be delayed to come after the x-ray signals. The same is true for all of the time spectra shown in Figs. 3–10. At first glance these two sets of recorded spectra look similar, and the spectra are typical of those observed for the other projectiles and charge states investigated in this work. Differences between the spectra and the other projectile-target systems measured are seen when gates are set on either the x-ray or particle spectra, thereby revealing coincidences with the individual outgoing charge states. For the C target spectra, it is noted that x-ray coincidences with the main beam are also measured, something that cannot be done with the gas targets.

In Fig. 3 are shown the sums of the collected x-ray singles events [Fig. 3(a)], the x-ray and doubly charge-changed, q-2 [Fig. 3(b)], and the x-ray and singly charge-changed, q-1 [Fig. 3(c)] coincidence events for 2.11 MeV/u F^{9+}+ N_2. Similar spectra (not shown) were obtained for F^{8+}+ N_2 and for F^{9+}, F^{8+} striking the Ne target. All of the spectra taken for F^{9+} and F^{8+} on N_2 and Ne were collected for $\sim 1.0 \times 10^{12}$ (taking about 3 weeks) incident particles, with measurements for each projectile charge state and target requiring about

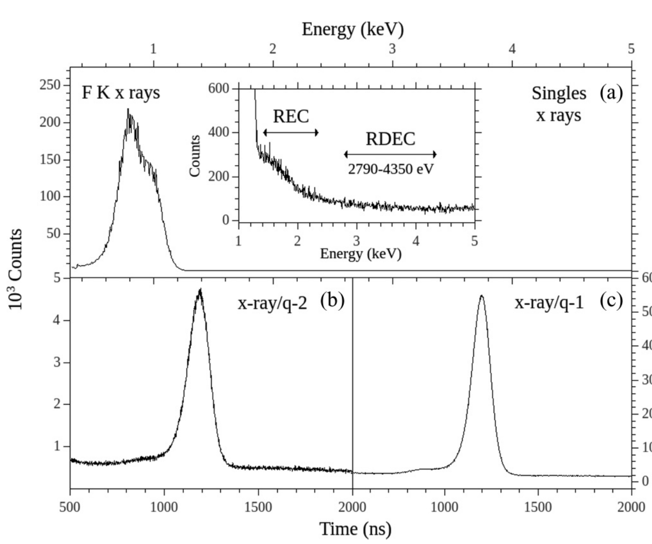

FIG. 3. Typical raw spectra obtained for the gas targets. Shown are the sums of collected (a) x-ray singles events, (b) x-ray and doubly charge-changed, q-2, and (c) x-ray and singly charged, q-1, coincidence events. The data are for 2.11 MeV/u (40 MeV) F^{9+}+ N_2. The RDEC range in eV is shown in the inset to (a).

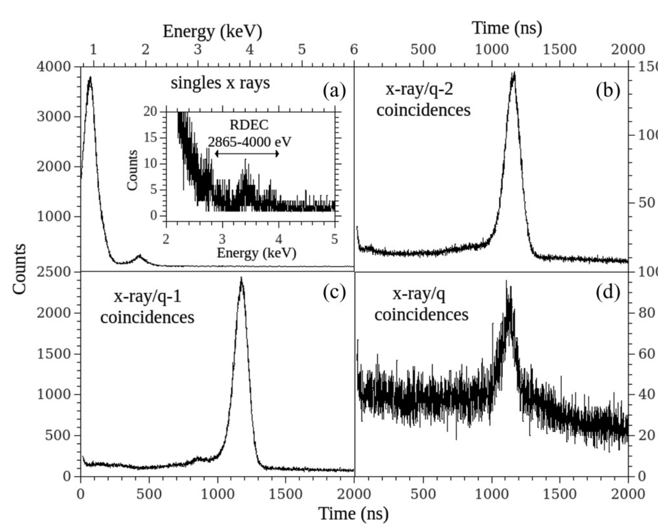

FIG. 4. Typical raw spectra obtained for the thin-foil C targets. Shown are the sums of collected (a) x-ray singles events, (b) x-ray and doubly charge-changed q-2, (c) x-ray and singly charged q-1, and (d) x-ray and no charge changed q coincidence events. The data are for 2.11 MeV/u (40 MeV) F^{9+}+ C. The RDEC range in eV is shown in the inset to (a).

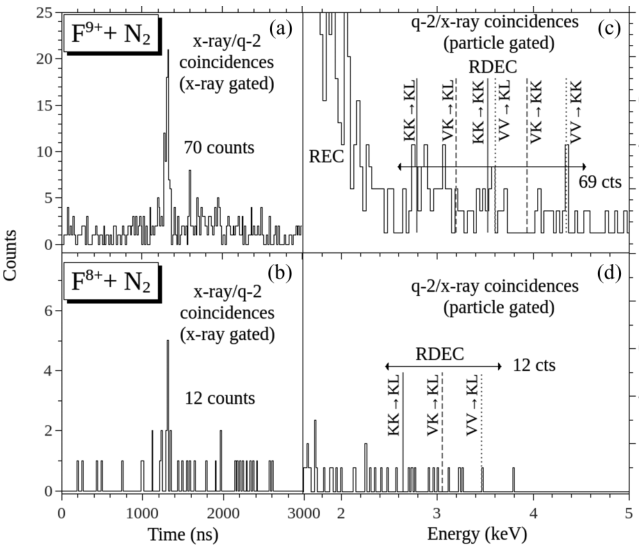

FIG. 5. Spectra obtained for 2.11 MeV/u (40 MeV) F^{9+} and F^{8+}+ N_2: (a), (b) the x-ray-gated particle spectra for the doubly charge-changed projectiles sorted using the region labeled RDEC in Fig. 3(a), while (c) and (d) are the particle-gated x-ray spectra corresponding to (a) and (b), respectively, i.e., the doubly charge-changed, q-2, outgoing state. The numbers shown on each graph are the totals for each spectrum after background subtraction, showing that the left and right panels agree with each other. The total number of incident particles was $\sim 1.0 \times 10^{12}$.

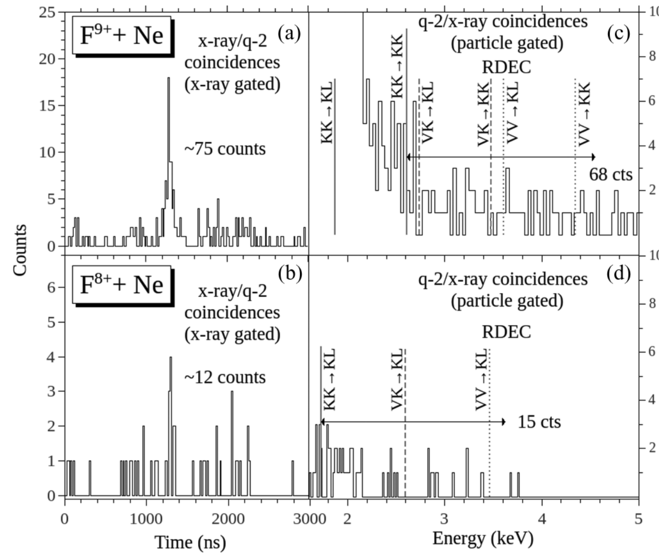

FIG. 6. Spectra obtained for 2.11 MeV/u (40 MeV) F^{9+} and F^{8+}+ Ne. See Fig. 5 for the rest of the caption. Please note these spectra were obtained for an RDEC region similar to that indicated in Fig. 5, which was taken from the Ne spectrum corresponding to Fig. 3(a).

500 h of collection time. The low number of incident particles ($\sim 10^{12}$) collected in 500 h for F^{9+} and F^{8+} is because the particle detectors can count efficiently only up to about 50 000 counts per second. The detector collecting the one-electron ions always had the highest count rate, so the beam was held to keep the rate on this detector to about this number. Figure 4 gives similar information as Figs. 3(a)–3(c), and in addition shows the x-ray and particle coincidences for outgoing particles with the same charge as the main beam q [Fig. 4(d)] for 2.11 MeV/u F^{9+}+ C. Similar spectra (not shown) were obtained for F^{8+}+ C, and for O^{8+} and O^{7+}+ C targets. For the thin-foil C data, spectra were collected for 7.13×10^9, 2.48×10^9, 3.74×10^9, and 2.11×10^9 incident particles, respectively, for the F^{9+}, F^{8+}, O^{8+}, and O^{7+} ions, with the measurements for each projectile charge-state and target system requiring 2–3 days of collection time. Thus, the thin-foil C targets took about 2 weeks to collect all of the data for the projectile-target systems investigated.

The spectra of Figs. 3 and 4, and the spectra like them for the other projectile charge states and targets studied, can then be used to generate x-ray-gated particle spectra and particle-gated x-ray spectra, which should give similar results for the numbers of events for each projectile-target system. Figures 5 and 6 show these results for the F^{9+} and F^{8+} projectiles on N_2 and Ne targets, respectively, for the data obtained, while Figs. 7 and 8 show the same information for $F^{9,8+}$ incident on thin-foil C and Figs. 9 and 10 show the same for $O^{8,7+}$ incident on C, respectively. For the gas targets, only the q-2 spectra are shown because, as mentioned above, it is only these spectra that can have a change of two in producing RDEC events. Double-capture events can occur in the x-ray range due to

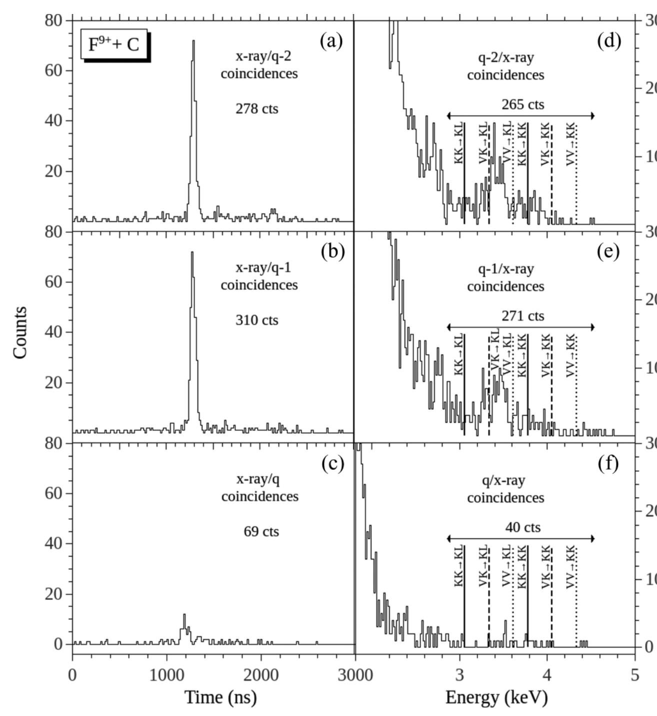

FIG. 7. Spectra obtained for 2.11 MeV/u (40 MeV) F^{9+}+ C: (a)–(c) the x-ray-gated particle spectra for the doubly, singly, and no charge-changed projectiles sorted using the region labeled RDEC in Fig. 4(a). (d)–(f) The particle-gated x-ray spectra corresponding to (a), (b), and (c), respectively, i.e., doubly, singly, and no charge-changed outgoing states. The numbers on each graph are the totals for each spectrum after background subtraction, showing that the left and right panels agree with each other. The total number of incident particles was $\sim 7.13 \times 10^9$.

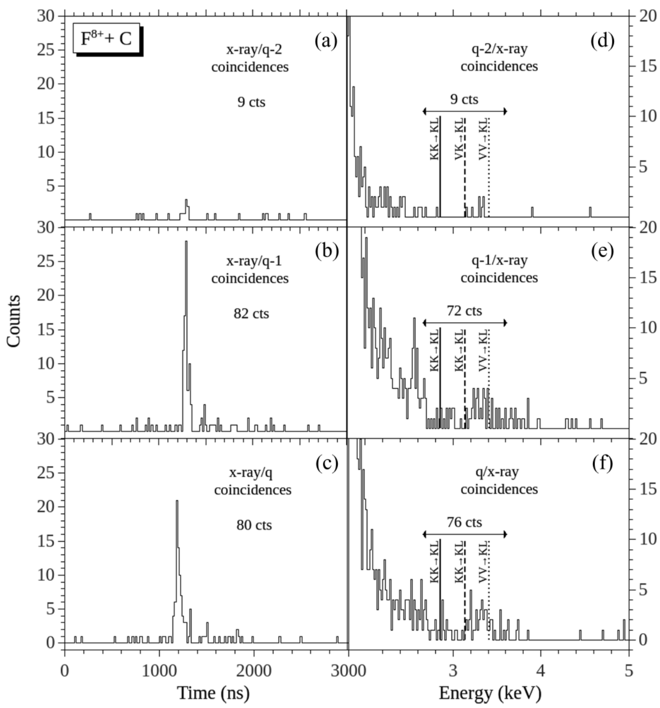

FIG. 8. Spectra obtained for 2.11 MeV/u (40 MeV) F^{8+}+ C: (a)–(c) X-ray-gated particle spectra for the doubly, singly, and no charge-changed projectiles sorted using a region similar to that labeled RDEC in Fig. 4(a). (d)–(f) Particle-gated x-ray spectra corresponding to (a), (b), and (c), respectively, i.e., doubly, singly, and no charge-changed outgoing states. The numbers shown on each graph are the totals for each spectrum after background subtraction, showing that the left and right panels agree with each other. The total number of incident particles was $\sim 2.48 \times 10^9$.

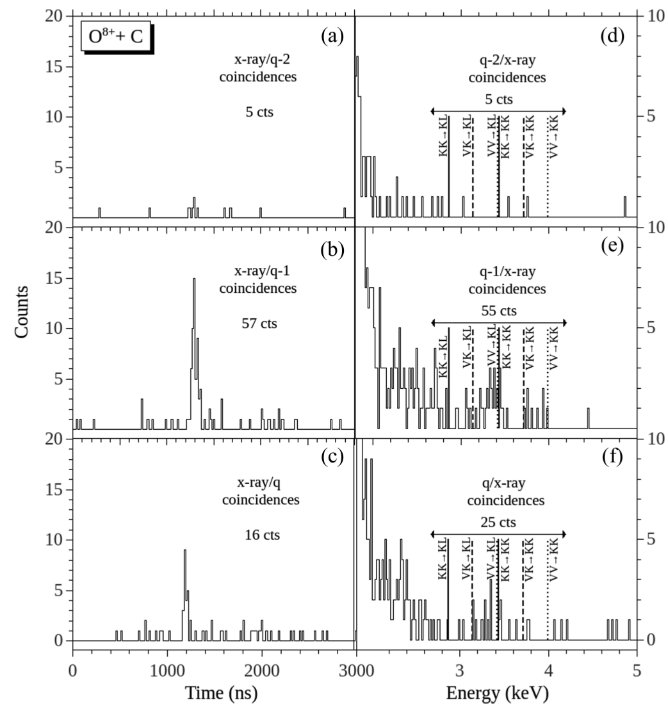

FIG. 9. Spectra obtained for 2.19 MeV/u (35 MeV) O^{8+}+ C: (a)–(c) X-ray-gated particle spectra for the doubly, singly, and no charge-changed projectiles sorted using a region similar to that labeled RDEC in Fig. 4(a). (d)–(f) Particle-gated x-ray spectra corresponding to (a), (b), and (c), respectively, i.e., doubly, singly, and no charge-changed outgoing states. The numbers shown on each graph are the totals for each spectrum after background subtraction, showing that the left and right panels agree with each other. The total number of incident particles was $\sim 3.74 \times 10^9$.

two REC events (see Fig. 3 above) in the q-2 spectra and can be seen from the x-ray gated particle spectra, as shown in Ref. [1], Figs. 3 and 4.

In comparing the spectra observed for the gas targets and the C foil, an obvious question is what role multiple collisions play in the foil data. For the gas target data these collisions do not occur because the measurements were done under single-collision conditions with a maximum of 5% of the incident beam changing charge in interactions with the target. On the other hand, for the foil targets (nearly) all of the incident particles have varying degrees of probability of undergoing charge-changing interactions due to the large stripping cross sections occurring in the relatively thick C-foil targets compared to the gas. These charge-stripping cross sections have the effect of changing the charge state formed in the RDEC process as the beam continues to move through the rest of the foil. This effect will be looked at in detail in the Discussion section below.

In Figs. 5 and 6, significant differences are seen in the numbers of events for F^{9+} and F^{8+}, a result attributed to the difference in K-shell vacancies in the projectile (two versus one) and, consequently, the allowed RDEC transitions. The number of counts (less background) in Figs. 5(a) and 5(c) and in 5(b) and 5(d) agree with each other, respectively, as do the counts in Figs. 6(a) and 6(c) and 6(b) and 6(d), but the events in Figs. 5(a) and 5(b) and 6(a) and 6(b) show these numbers most clearly. Moreover, Figs. 5(c) and 6(c) give some insight into which RDEC transitions (see Table I) occur. The numbers of events in Figs. 5(b) and 6(b) are so few that, while peaks can be seen in these x-ray-gated particle spectra, peaks cannot be seen in the particle-gated x-ray spectra of Figs. 5(d) and 6(d) due to the three expected transitions (see Table I for F^{8+} on the N_2 and Ne targets) in these latter figures. Also, the particle events in Figs. 5(a) and 5(b) and 6(a) and 6(b) result in sharper peaks at higher channel numbers than the particle events shown in Fig. 3(b). Both the sharper peak and higher channel numbers are due to the excellent time resolution of the x-ray detector used in these measurements, resulting in electronic signals with sharper rise times due to differences in the pulse height.

Figure 7 shows essentially the same information as Figs. 5 and 6 for the particle and x-ray spectra for F^{9+} ions incident on C, the difference being that x-ray spectra are shown for each accompanying outgoing charge state to its immediate left. Figure 8 shows this information for F^{8+} on C, while Figs. 9 and 10 display the information for O^{8+} and O^{7+} on C. In comparing these C-foil spectra, large differences are seen depending which of the four incident projectiles are involved and which outgoing charge state of the projectile is considered. This dependence on outgoing charge state is very different from what is found for gas targets as shown in Figs. 5 and 6 above.

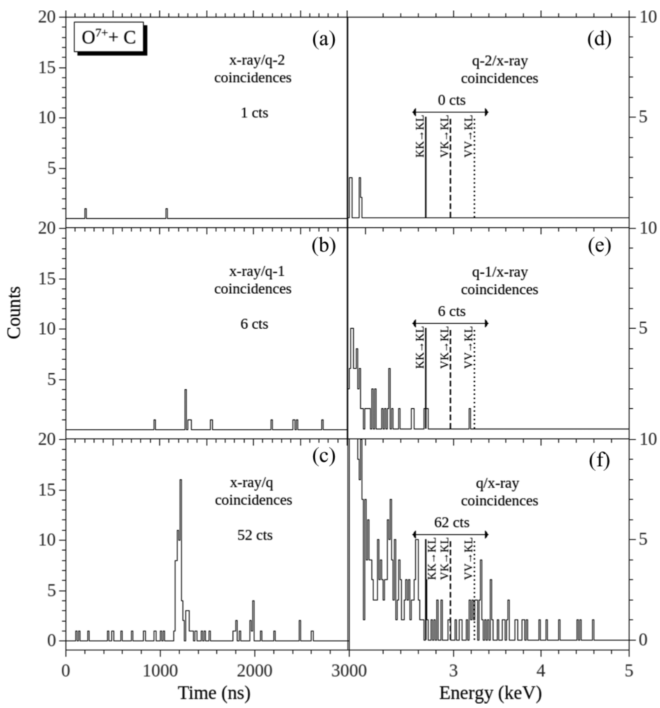

FIG. 10. Spectra obtained for 2.19 MeV/u (35 MeV) O^{7+}+ C: (a)–(c) the x-ray-gated particle spectra for the doubly, singly, and no charge-changed projectiles sorted using a region similar to that labeled RDEC in Fig. 4(a). (d)–(f) The particle-gated x-ray spectra corresponding to (a), (b), and (c), respectively, i.e., doubly, singly, and no charge-changed outgoing states. The numbers shown on each graph are the totals for each spectrum after background subtraction, showing that the left and right panels agree with each other. The total number of incident particles was $\sim 2.11 \times 10^9$.

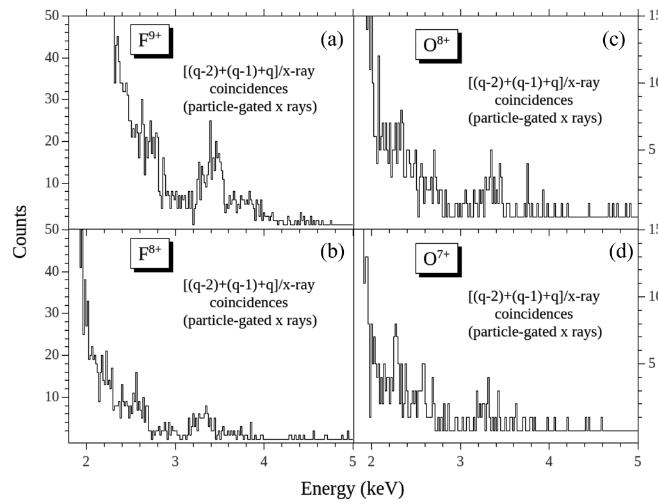

FIG. 11. Particle-gated x-ray spectra for the sum of q-2, q-1, and q outgoing charge states of incident 2.11 MeV/u (40 MeV) $F^{9,8+}$ and 2.19 MeV/u (35 MeV) $O^{8,7+}$ projectiles on C: (a), (b) are for F^{9+} and F^{8+}, respectively, and (c) and (d) for O^{8+} and O^{7+}, respectively. The total number of incident particles is given by the numbers in Figs. 7–10.

Figure 11 shows the sums of the x-ray spectra in Figs. 7–10. These spectra represent the sums of the particle-gated x-ray spectra for q-2, q-1, and q outgoing charge states of F^{9+}, F^{8+}, O^{8+}, and O^{7+} on C, respectively, shown in Figs. 7(d)–7(f), 8(d)–8(f), 9(d)–9(f), and 10(d)–10(f). The differences between the spectra for the C-foil target and those for the gas targets imply large charge stripping cross sections resulting in multiple collisions in the foil targets that do not exist for the gas targets that were done under single-collision conditions. This will be discussed in the following section.

In reviewing these figures for RDEC and the charge-changing associated with them, large differences are seen in the results for gas targets and C-foil targets, as well as in the results for the two different ion species and the respective charge states considered. For the gas targets, RDEC only appears in the doubly charge-changed, q-2, outgoing channel, while for the C-foil RDEC events appear in all three outgoing charge state channels q-2, q-1, and q. Also, the differences in RDEC findings between the fully stripped and one-electron projectiles are nearly a factor of 6 for the gas targets, while for C-foil targets normalized to the incident beam current, this difference is much smaller, coming to about the same value. Moreover, examination of the outgoing charge-state C-foil spectra individually for fully stripped and one-electron fluorine and oxygen projectiles shows that the two projectiles give very different results for RDEC, with the spectra for oxygen shifting to significantly higher outgoing charge states than the fluorine ions. These different findings in the results between oxygen and fluorine ions occur despite the fact that the ionic species are just one atomic number apart. The causes, including the effects of the multiple collisions that inevitably occur in the C-foil target measurements, will be explored more in Sec. V immediately following.

V. DISCUSSION

In this section we will first discuss the effects of multiple collisions on RDEC and what they cause in determining the cross sections. While the gas and foil targets are expected to give values for the RDEC cross sections that are at least similar, these targets also yield quite different findings for the outgoing charge states in which the RDEC events result in the multiple collisions for the case of the thin-foil targets. The discussion will begin with the effects of single and multiple collisions by the ions as they transverse the target following the formation of an RDEC event. This will be followed by comments on the equilibrium of the charge distribution of the ion beam as it moves through the foil. Then the determination of the measured differential cross sections at 90° and the calculation and assumptions that go into obtaining total cross sections from the differential cross sections will be presented. This discussion will also include comparison with the available theoretical cross sections for the systems studied. The section will conclude with comments on the large difference between the cross sections of fully stripped and one-electron projectiles striking the gas targets, and reasons for less of a difference in the case of the foil targets.

A. Single and multiple collisions in RDEC

Here, the differences between the gas targets and the C foil are discussed. For gas targets the measurements are easily

TABLE II. Estimated charge-stripping cross sections for ∼2 MeV/u highly stripped oxygen and fluorine on carbon. The O^{q+} and F^{q+} cross sections were scaled from Refs. [17–19], respectively. By applying the cross sections to the relevant charge states of Figs. 7–10, the relative distributions of the q-2, q-1, and q spectra are readily seen.

O^{q+}+ C	Cross section (Mb)	F^{q+}+ C	Cross section (Mb)
5+ → 6+	19.0	6+ → 7+	4.0
6+ → 7+	3.6	7+ → 8+	1.0
7+ → 8+	0.4	8+ → 9+	0.2

carried out under single-collision conditions by adjusting the gas pressure in the target cell, while for the C-foil targets this cannot be done. All of the gas target measurements were carried out with target densities (∼10 mTorr ∼3.3× 10^{14} atoms/cm^3) such that less than 5% of the incident beam changed charge in passing through the target. For the C-foil targets, the densities (about 15 μg/cm^2 = 7.53 × 10^{17} atoms/cm^2) were such that single-collision conditions are not possible. This difference between the single- and multiple-collision conditions can be expected to lead to very different results in the outgoing charge-state channels in which RDEC events occur. In the latter case, the multiple collisions lead to a change in the charge of the incident ion as it continues passage through the foil following the RDEC process. This occurs by assuming RDEC occurs on average halfway through the foil following which half of the foil can still be used for charge changing. This charge change is most likely caused by subsequent stripping of the ion that underwent RDEC.

Table II shows the estimated charge stripping cross sections for fully stripped and one-electron $O^{8,7+}$ and $F^{9,8+}$ projectiles [17–19] that have undergone RDEC. Multiplying these cross sections by half the foil thickness (∼4 × 10^{17} atoms/cm^2), the average distance the passing ion still has to travel, the probabilities of the relative distributions of the charge states obtained in Figs. 7–10 are predicted. It should be recalled that a probability of more than unity implies that the process of charge stripping almost certainly takes place, while a value less than unity means that approximately the calculated fraction changes charge in passage through the foil. With these facts in mind, the probabilities are 7.5, 1.4, and 0.16 for oxygen projectiles undergoing stripping for the charge states 5+ → 6+, 6+ → 7+, and 7+ → 8+ are obtained, respectively; hence, the charge states 5+ and 6+ formed following the RDEC process for one-electron and fully stripped ions (Figs. 10 and 9, respectively) are most likely to change their charge, while those that reach 7+ have a smaller probability to change.

For fluorine projectiles these probabilities work out to 1.6, 0.4, and 0.08 for the stripping processes 6+ → 7+, 7+ → 8+, and 8+ → 9+, respectively; hence, for fluorine only the 6+ charge state formed in the RDEC process likely changes charge with certainty (Fig. 8), while those formed as 7+ (Fig. 7) have about an even chance of stripping further and those that go to the 8+ state have little chance of changing charge.

So, these probabilities show quite clearly the differences between the relative charge-state distributions of oxygen and fluorine ions, as well as the effect of the differences between their initial charge states. These probabilities can be compared with the charge distributions displayed in Figs. 7–10, panels (a)–(c).

It is also noted that charge stripping can occur prior to an RDEC event. For O^{7+} ion stripping occurs to charge state 8+ and for F^{8+} it occurs to 9+. From Table II this happens about 32% of the time for O^{7+} and 16% of the time for F^{8+}. In this case, a fraction of the O^{7+} and F^{8+} beams are lost for RDEC, becoming O^{8+} and F^{9+} ions instead. Hence, the numbers of photons associated with these incident ions should not be included, but rather the photons from O^{8+} and F^{9+} RDEC should be subtracted from the total RDEC intensity observed for O^{7+} and F^{8+}. These corrections have been made to the cross sections listed for O^{7+} and F^{8+} (see Table IV), including the uncertainty associated with each ion, which is taken to be ±40% for O^{8+} and ±30% for F^{9+}. The disadvantage of not counting charge-changed O^{8+} and F^{9+} for initial beams of O^{7+} and F^{8+} is that the actual fraction of charge-stripped ions is not measured (see Fig. 2) and, hence, the fraction must be estimated from the table of reported stripping cross sections.

B. Equilibrium charge-state distributions

For the gas targets the outgoing charge distribution of the ion beam has no effect on the RDEC process because the pressure was set for single-collision conditions. In this case, the pressure was always such that less than 5% of the incident beam changed charge in passage through the target. Hence, the doubly charge-changed (q-2) channel formed in the RDEC process is the only one that needs to be considered, as shown in Figs. 5 and 6. The singly charge-changed (q-1) channel was also observed and no RDEC events were seen. Such is not the case for the foil targets, however.

For the thin-foil C targets the probability that the charge distribution is not in equilibrium has been observed for REC events [20]. The foil thickness in this work for RDEC is near the beginning of the fraction vs thickness curve (T ∼ 0), where the REC cross section obtained is equal to the desired value and the charge has not changed appreciably (see Fig. 3 of Ref. [20]). If the same assumption holds for RDEC, then the values obtained for the cross sections should also be close to the “zero-thickness” value. If this is so, then the effects of nonequilibrium of the charge distribution do not need to be considered, and the small divergence from equilibrium can be taken into account in the overall uncertainties assigned to the cross sections.

C. Calculation of the RDEC cross sections

Determination of the differential cross sections at 90° for F^{9+} and F^{8+} incident on the gas targets N_2 and Ne is straightforward and can be calculated from the RDEC counts observed in the q-2 outgoing charge state channel, the total number of incident particles, the gas pressure used, the solid angle subtended by the x-ray detector, and the efficiency of the x-ray detector. Only the differential cross sections are obtained from the measurements and the total RDEC cross sections are then calculated assuming polarization of the RDEC events is the same as REC events [14,15].

In determining values for the cross sections for the foil targets measured, two rather strong contamination lines are seen in the x-ray spectra of Figs. 7–10 near 3.4 and 3.8 keV for each of the outgoing charge states associated with the four projectile charge states and also in the total x-ray spectra of Fig. 11 for the summed spectra of Figs. 7–10. These lines are attributed to contamination by potassium and calcium. The origin of these lines is not known, but they have been observed before in our measurements for fluorine ions on thin C [11], and might have come from improper handling of the foils prior to their installation in the target chamber; however, every step was taken to avoid this mishandling. The intensities of these contamination lines must be taken into account and corrected for in order to get reasonable values for the differential RDEC cross sections. These differential cross sections can then be converted to total RDEC cross sections assuming the polarizability [14,15] of the x rays is the same as that for the REC lines.

Corrections for the contaminant lines were done by generating additional particle-gated x-ray spectra (not shown) corresponding to a region encompassing these two peaks from about 3.3 to 4.0 keV (see Fig. 11). However, the full contribution of the contaminant lines cannot be subtracted from the RDEC region without underestimating the values of the cross sections. So, the number of counts to be subtracted for each incident ion were determined by normalizing the contaminant counts to the "background" RDEC intensity. In this way the extent of the reduction in the contaminant peak required could be found, and these factors were 0.35, 0.33, 0.25, and 0.25 for F^{9+}, F^{8+}, O^{8+}, and O^{7+}, respectively. The uncertainties in making these corrections were taken to be 20% for the fluorine projectiles and 25% for the oxygen projectiles and these values were included in determining the error bars for the calculated cross sections.

As mentioned before, only differential cross sections at 90° were measured in this work. From the information determined, these differential cross sections can be calculated from the relation

$$\frac{d\sigma_{\rm RDEC}}{d\Omega}(\theta = 90^\circ) = \frac{N_{\rm RDEC}}{I_o}\frac{1}{T\,\Delta\Omega\epsilon}, \tag{4}$$

where $N_{\rm RDEC}$ is the number of RDEC events measured, I_o is the total number of incident ions, T is the target thickness (in atoms/cm^2), $\Delta\Omega$ is the solid angle (in steradians) subtended by the x-ray detector, and ϵ ($\sim$1) is the detection efficiency of the x rays. If the angular dependence between the RDEC differential cross sections and the corresponding REC cross sections goes as $\sin^2\theta$ [14,15], then the total cross sections can be determined by multiplying this equation by $8\pi/3$ as shown by Eq. (3) above in Sec. II.

Table III shows the differential cross sections for RDEC calculated from Eq. (4) and the total cross sections for RDEC determined from Eq. (3) for the gas targets, while Table IV lists the differential and total RDEC cross sections for the C thin-foil targets used. The cross sections of Tables III and IV are plotted in Fig. 12. The differential cross sections are shown in the upper parts of the plot and the total cross sections (assuming a $\sin^2\theta$ dependence with the differential) are shown in the lower parts. The gas target results are shown in the leftmost panels and the thin-foil cross sections are in the rightmost panels. The cross sections for the gas targets are smaller in general than those for the C-foil target, with the cross sections for the fully stripped ions differing by a factor of nearly 6 from the cross sections for the one-electron ions.

TABLE III. RDEC differential and total (differential multiplied by $8\pi/3$) cross sections (in barns/steradian/atom and barns/atom, respectively) for the four systems of 2.11 MeV/u (40 MeV) fluorine ions incident on gas targets of N_2 and Ne. The numbers in parentheses following each cross section represent the uncertainty in the value obtained.

	$F^{9+}+N_2$	$F^{8+}+N_2$	$F^{9+}+$ Ne	$F^{8+}+$ Ne
$\frac{d\sigma}{d\Omega}(\theta=90^\circ)$	0.30(0.17)	0.05(0.03)	0.25(0.14)	0.039(0.024)
$\sigma_{\rm total}$	2.5(1.4)	0.42(0.25)	2.1(1.2)	0.33(0.20)

The most recent, and believed to be the best so far, theoretical total cross sections [21] are shown by the open squares and circles, and these exist only for the thin-foil targets. Calculations were not performed for the gas targets used in this work. These theoretical cross sections were calculated using the line-profile approach by two methods, labeled as the A model and the K model by the authors of the reference. In the A model a homogeneous electron density was assumed for the entire target atom and all electrons were included in the calculations. In the K model only the target K electrons were included and a homogeneous electron density was assumed for the K shell. The theoretical values, calculated for the total cross sections, are seen to disagree substantially with the measured values, with the results of the A model being the closest. A possible error in this model could be the assumption of a homogeneous electron density for the entire atom. In this way, the effect of all of the electrons might be underestimated, therefore giving rise to theoretical cross sections that are too small.

Other theoretical calculations [22–24] show poorer agreement with the measurements and are not included in the comparison, except for the theory points from Mikhailov *et al.* [24] for O^{8+} and $F^{9+}+$ C, shown by the open diamonds in the lower part of the C-foil results. These points are seen to dramatically underestimate the measured cross sections.

The cross sections for fully stripped oxygen and fluorine ions determined from the present measurements agree fairly well with the previous values, but in all cases are smaller. For O^{8+} the previous value found for the differential cross

TABLE IV. RDEC differential and total (differential multiplied by $8\pi/3$) cross sections (in barns/steradian/atom and barns/atom, respectively) for the four systems of 2.19 MeV/u (35 MeV) oxygen and 2.11 MeV/u (40 MeV) fluorine ions incident on thin-foil targets of carbon. The numbers in parentheses following each cross section represent the uncertainty in the value obtained.

	$O^{8+}+$ C	$O^{7+}+$ C	$F^{9+}+$ C	$F^{8+}+$ C
$\frac{d\sigma}{d\Omega}(\theta=90^\circ)$	0.24(0.06)	0.24(0.10)	1.0(0.2)	0.66(0.20)
$\sigma_{\rm total}$	2.0(0.5)	2.0(0.8)	8.4(1.7)	6.6(1.5)

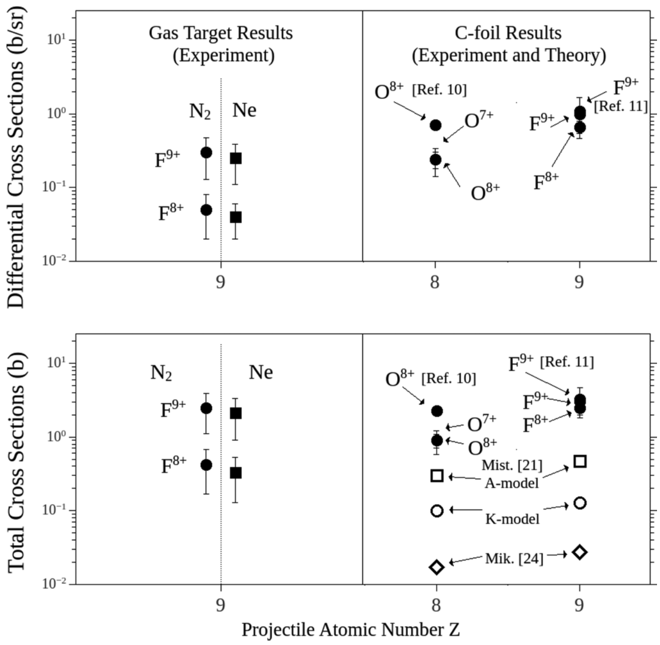

FIG. 12. Present results for F^{9+} and F^{8+} projectiles incident on gas targets (N_2 and Ne), and for these same projectiles in addition to O^{8+} and O^{7+} incident on thin-foil C targets. The present gas results are in the leftmost panels and the thin-foil results in the rightmost panels. Theoretical calculations of Refs. [21,24] are also shown, which were only done for the foil targets.

section was 0.71(0.5) and for F^{9+} it was 1.1(0.6) barns. In this work, cross sections for the C-foil target are reported for one-electron projectile ions. These cross sections do not differ greatly from those for the bare ions, contrary to the results previously found for F^{9+} and F^{8+} ions on gas targets under single-collision conditions where the difference is about a factor of 6. This large contrast is attributed to the effect of multiple collisions for the projectile ions incident on thin-carbon foils. Additional theoretical cross-section calculations should help to shed more light on the RDEC process and provide insight into the differences between single- and multiple-collision conditions.

D. Inconsistencies between gas and thin-foil RDEC cross sections

Examination of the RDEC cross sections for the gas targets shown in Figs. 5 and 6 (for N_2 and Ne, respectively) and listed in Table III shows the fully stripped ions with about six times larger values than the cross sections for one-electron ions. On the other hand, the data for the thin-foil targets show something quite different, with fluorine having cross sections for the fully stripped ion about 20% larger than the one-electron ion cross sections (see Table IV). The results for oxygen ions show the fully stripped and one-electron projectile values to have about the same value (see Table IV). This situation appears difficult to understand. It is probably easier to explain the large differences between the two charge states used for the gas targets than the relatively small separation found for the foil targets. Thus, the gas targets will be considered first.

As noted above, the difference in the RDEC gas target cross sections for both N_2 and Ne was about a factor of 6 with the cross sections for the fully stripped projectiles being larger (see Table III). For the one-electron projectiles an electron is already present in the K shell, so it can be said that the probability for RDEC transitions is reduced by at least a factor of 2. But this cannot be the entire story because two electrons are involved in every RDEC transition, so the spin of the two incoming electrons must be considered. Since there is already one electron in the K shell, an electron filling the other vacancy must have a spin opposite to the one that is there. The incoming electrons are captured as a pair and these likely both have spins in the S state, which can be either a singlet (^1S) or a triplet (^3S). The singlet state has an aligned and unaligned electron with the existing K-shell electron, and hence likely reduces the one-electron ion cross section by another factor of 2 compared to the fully stripped ions. For the triplet state, two of the electrons have aligned configurations, and are thus forbidden from making the transition, while the other two are unaligned and can transfer to the K shell. This would likely reduce the cross section even more, thereby permitting a reduction to possibly a factor of 6. Unfortunately, the resolution and statistics of the lines in the RDEC x-ray spectra obtained for the present data (Figs. 5 and 6) are insufficient for determination which of these possibilities is more likely to occur. Hence, a detailed analysis of the transitions that are possible cannot be presented but only point in the general direction, as done here, in which the transitions go. For the fully stripped projectiles this situation does not come up and the transition of electrons from the target via the singlet or triplet states is entirely possible.

For the thin-foil targets, the charge state of ions with one or two initial K-shell vacancies is easily changed by stripping a newly formed RDEC event in passage through the remainder (on average half the thickness) of the foil. This can be seen from the particle spectra of Figs. 7–10 and from Table II which lists the charge-stripping cross sections of the charge states formed in the RDEC process. These charge-stripping cross sections are of such a size that most collisions have large probabilities of changing the charge state of the ion that just underwent RDEC. It is likely that these charge-stripping events result in the ions losing their sensitivity to the spin states of the incoming two electrons, and so the spins make little difference in whether an electron is stripped or not. Thus, the explanation seems to be in the thickness of the target that unavoidably leads to multiple collisions. The gas targets do not suffer multiple collisions and thus maintain their charge state following RDEC in passage through the remainder of the gas target. For the foil targets studied, the projectiles studied only rarely maintain the charge formed during RDEC (see Figs. 7–10), and thus appear in an elevated charge state as seen from the small probabilities of the unchanged charge states.

These explanations leave something further to examine, but they are an attempt to understand the reason for the seemingly fixed factor of nearly 6 for the fully stripped RDEC cross sections compared to the one-electron ions in gas targets, while no such factor seems to exist for the foil target results. Better data with more statistics and improved resolution could help to answer these questions, likely a long and arduous task.

VI. CONCLUSION

Radiative double-electron capture was investigated for fully stripped and one-electron ions of fluorine in collisions with gas targets of N_2 and Ne, while thin-foil targets of carbon were investigated for fully stripped and one-electron ions of oxygen and fluorine. The thin-foil targets were a followup to our earlier studies for oxygen and fluorine that showed some evidence for RDEC but were not definitive. The gas targets were undertaken to verify the existence of RDEC and to measure the cross sections for the process without the complications of multiple collisions. These measurements were followed by more complete investigations of RDEC for thin-foil carbon, and in these studies RDEC was seen in the doubly charge-changed channel (expected), the singly charge-changed channel, and the no change in charge channel. In the earlier measurements [10], the no charge channel was not measured as it was believed that no RDEC events would appear in this channel. Also, the one-electron incident ions were not studied [11] since previous measurements seemed not to show RDEC events for this ion. This last case turned out not to be true, and, furthermore, significant numbers of events were seen in the no charge channel for both ions in both charge states. For the gas targets, RDEC events were only observed in the doubly charge-changed channel as expected.

Cross sections were determined for both the fully stripped and one-electron fluorine ions incident on the gas targets, and for the thin-foil targets the same fluorine ions, in addition to fully stripped and one-electron oxygen ions, were investigated. In all cases, the cross sections for all of the projectiles studied were not too different from one another, with the cross sections for fully stripped fluorine striking the gas targets being about four times smaller than those found for the thin-foil carbon. For the foil targets with the fluorine and oxygen projectiles the cross sections determined are about an order of magnitude larger than the most recent and seemingly best theoretical cross sections. The experimental cross sections were assumed to have a $\sin^2\theta$ dependence between the measured differential cross sections at 90° and the predicted total cross sections, so this observation is based on the extent to which this assumption is valid.

A major difference between the gas targets and the thin-foil targets is the fact multiple collisions occur for foil targets. These collisions are mainly due to charge-stripping resulting in the outgoing charge being elevated, so the majority of the RDEC events can be found in the singly charge-changed or the no charge-changed channels. For the gas targets, no such charge changing occurs. Furthermore, in the case of the gas targets the difference between the fully stripped and one-electron ions is about a factor of 6 with the fully stripped ions having the larger cross sections. For the foil targets, the cross sections for the fully stripped and one-electron ions are quite comparable. Also, the one-electron ions have to be corrected for stripping to fully stripped ions in passage through the foil. The estimated contribution of photons to the incident one-electron ion cross sections for $O^{7+} \rightarrow O^{8+}$ and $F^{8+} \rightarrow F^{9+}$ is then subtracted from the events found for the total section, thereby giving larger uncertainties in these one-electron cross sections.

To explain the differences between the gas and foil-target cross sections, the spin statistics for the gas targets of the incoming electrons and the compatibility of them with a one-electron ion must be taken into account, and, while the statistics and resolution of the two captured electrons cannot be observed in the x-ray spectra obtained, a factor of about 6 can be accounted for. For the thin-foil target, the compatibility of the incoming electrons does not seem to play a role and is it reasonable to assume these conditions are broken.

In summary, this work represents a fairly complete study of RDEC for fully stripped and one-electron projectiles incident on gas and thin-foil targets. There is also some comparison with theoretical calculations but this consideration is not complete because there are no results for the projectile-gas targets done in this study. Future work could focus on the angular dependence of RDEC to see if a $\sin^2\theta$ relationship holds between the differential cross sections at 90° and the total cross sections. Also, the study of a helium target would be worthwhile as this target has just two electrons, which means only two transitions are possible, namely, $KK \rightarrow KK$ and $KK \rightarrow KL$ (only the $KK \rightarrow KL$ would be possible for F^{8+} projectiles). However, the emission polarization and the helium target studies would require much beam time and great effort, so a real commitment would be needed to undertake either one of these studies. In fact, observation of RDEC in helium was attempted, giving only three RDEC counts in about 10 days of round-the-clock beam time. Hence, this target was abandoned in favor of running the more count-productive N_2 and Ne targets. Finally, more theoretical work should be done to determine why the present calculations are off by about an order of magnitude and also calculations are needed to compare the theory with the present gas target measurements. Such studies could provide much needed insight into the process of RDEC.

ACKNOWLEDGMENTS

This work was supported in part by National Science Foundation Grant No. PHY-1707467. The authors are very grateful to Professor A. Kayani for his help in making the accelerator available and for keeping it running. Our thanks also go to A. Kern for his expert help with the technical equipment associated with the accelerator facility and to R. Welch and J. Byers, the department instrument makers. Finally, we also wish to thank P. Niraula and S. Iqbal, along with S. Buglione, C. McCoy, C. Taylor, and J. White, who participated in the early data taking phases of the experiment.

[1] D. S. La Mantia, P. N. S. Kumara, S. L. Buglione, C. P. McCoy, C. J. Taylor, J. S. White, A. Kayani, and J. A. Tanis, Phys. Rev. Lett. **124**, 133401 (2020).

[2] D. S. La Mantia, P. N. S. Kumara, C. P. McCoy, and J. A. Tanis, Phys. Rev. A **102**, 060801(R) (2020).

[3] H. W. Schnopper, H. D. Betz, J. P. Delvaille, K. Kalata, A. R. Sohval, K. W. Jones, and H. E. Wegner, Phys. Rev. Lett. **29**, 898 (1972).

[4] T. Stöhlker, C. Kozhuharov, P. H. Mokler, A. Warczak, F. Bosch, H. Geissel, R. Moshammer, C. Scheidenberger,

J. Eichler, A. Ichihara *et al.*, Phys. Rev. A **51**, 2098 (1995).
[5] J. Eichler and T. Stohlker, Phys. Rep. **439**, 1 (2007).
[6] J. Miraglia and M. S. Gravielle, *International Conference on Photonic, Electronic and Atomic Collisions XV: Book of Abstracts* (Springer, Boston, 1987), p. 517.
[7] A. Warczak, M. Kucharski, Z. Stachura, H. Geissel, H. Irnich, T. Kandler, C. Kozhuharov, P. H. Mokler, G. Muezenberg, F. Nickel *et al.*, Nucl. Instrum. Methods Phys. Res., Sect. B **98**, 303 (1995).
[8] G. Bednarz, D. Sierpowski, Th. Stoehlker, A. Warczak, H. Beyer, F. Bosch, A. Braeuning-Demian, H. Braeuing, X. Cai, A. Gumberidze *et al.*, Nucl. Instrum. Methods Phys. Res., Sect. B **205**, 573 (2003).
[9] A. V. Nefiodov, A. I. Mikhailov, and G. Plunien, Phys. Lett. A **346**, 158 (2005).
[10] A. Simon, A. Warczak, T. Elkafrawy, and J. A. Tanis, Phys. Rev. Lett. **104**, 123001 (2010).
[11] T. Elkafrawy, A. Warczak, A. Simon, and J. A. Tanis, AIP Conf. Proc. **1525**, 64 (2013); T. Elkafrawy, A. Simon, J. A. Tanis, and A. Warczak, Phys. Rev. A **94**, 042705 (2016).
[12] N. Winters, A. Warczak, J. A. Tanis, T. Gassner, A. Gumberidze, S. Hagmann, P. M. Hillenbrand, C. Kozhuharov, N. Petridis, and R. Reuschl, Phys. Scr. **T156**, 014083 (2013).
[13] F. Biggs, L. B. Mendelsohn, and J. B. Mann, At. Data Nucl. Data Tables **16**, 201 (1975).
[14] R. Anholt, S. A. Andriamonje, E. Morenzoni, Ch. Stoller, J. D. Molitoris, W. E. Meyerhof, H. Bowman, J.-S. Xu, Z.-Z. Xu, J. O. Rasmussen *et al.* Phys. Rev. Lett. **53**, 234 (1984).
[15] S. Tashenov, T. Stohlker, D. Banas, K. Beckert, P. Beller, H. F. Beyer, F. Bosch, S. Fritzsche, A. Gumberidze, S. Hagmann *et al.*, Phys. Rev. Lett. **97**, 223202 (2006).
[16] W. E. Meyerhof, R. Anholt, J. Eichler, H. Gould, C. Munger, J. Alonso, P. Thieberger, and H. E. Wegner, Phys. Rev. A **32**, 3291 (1985).
[17] T. R. Dillingham, J. R. Macdonald, and P. Richard, Phys. Rev. A **24**, 1237 (1981).
[18] S. A. Boman, E. M. Bernstein, and J. A. Tanis, Phys. Rev. A **39**, 4423 (1989).
[19] S. M. Ferguson, J. R. Macdonald, T. Chiao, L. D. Ellsworth, and S. A. Savoy, Phys. Rev. A **8**, 2417 (1973).
[20] J. A. Tanis and S. M. Shafroth, Phys. Rev. Lett. **40**, 1174 (1978).
[21] E. A. Mistonova and O. Y. Andreev, Phys. Rev. A **87**, 034702 (2013).
[22] V. L. Yakhontov and M. Y. Amusia, Phys. Lett. A **221**, 328 (1996).
[23] V. L. Yakhontov and M. Y. Amusia, Phys. Rev. A **55**, 1952 (1997).
[24] A. I. Mikhailov, I. A. Mikhailov, A. N. Moskalev, A. V. Nefiodov, G. Plunien, and G. Soff, Phys. Rev. A **69**, 032703 (2004).